Revision of Paschen's Law Relating to the ESD of Aerospace Vehicle Surfaces

Michael D. Hogue, PhD
NASA, Flight Technology Branch, UB-R2
Electrostatics & Surface Physics Laboratory
Kennedy Space Center, FL 32899
phone: (1) 321-867-7549
E-mail: Michael.D.Hogue@nasa.gov

Rachel E. Cox
NASA, Flight Technology Branch, UB-R2
Kennedy Space Center, FL 32899
E-mail: Rachel.E.Cox@nasa.gov

Jaysen Mulligan
University of Central Florida
Orlando, FL 32816
E-mail: mulligan2015@gmail.com

Jayanta Kapat, PhD
University of Central Florida
Orlando, FL 32816
E-mail: Jayanta.Kapat@ucf.edu

Kareem Ahmed, PhD
University of Central Florida
Orlando, FL 32816
E-mail: Kareem.Ahmed@ucf.edu

Jennifer G. Wilson
NASA, Flight Technology Branch, UB-R2
Kennedy Space Center, FL 32899
E-mail: Jennifer.G.Wilson@nasa.gov

Luz M. Calle, PhD
NASA, Applied Science Branch, UB-R3
Kennedy Space Center, FL 32899
E-mail: Luz.M.Calle@nasa.gov

Abstract— **The purpose of this work is to develop a version of Paschen's law that takes into account the flow of ambient gas past electrode surfaces. Paschen's law does not consider the flow of gas past an aerospace vehicle whose surfaces may be triboelectrically charged by dust or ice crystal impingement while traversing the atmosphere. The basic hypothesis of this work is that the number of electron-ion pairs created per unit distance between electrode surfaces is mitigated by the electron-ion pairs removed per unit distance by the flow of gas. The revised theoretical model must be a function of the mean velocity v_{xm} of the ambient gas and reduce to Paschen's law when the mean velocity is zero. A new theoretical formulation of Paschen's law, taking into account the Mach number and compressible dynamic pressure, derived by the authors, will be discussed. This equation has been evaluated by wind tunnel experimentation. Initial data of the baseline wind tunnel experiments show results consistent with the hypothesis. This work may enhance the safety of aerospace vehicles through a redefinition of electrostatic launch commit criteria. It is also possible for new products, such as antistatic coatings, to be formulated based on this data.**

TABLE 1: NOMENCLATURE

V_s	Sparking discharge voltage (V)
V_i	Ionization potential of the ambient gas (V)
L	Molecular mean free path at standard atmospheric pressure (6.8×10^{-6} cm)
P_{atm}	Atmospheric pressure at sea level (760 torr)
P	Total gas pressure (torr)
P_0	Ambient gas pressure (torr)
P_{DI}	Incompressible Dynamic Pressure (torr)
P_{DC}	Compressible Dynamic pressure (torr)
ρ	Gas density (Kg/m^3)
d	Electrode separation (cm)
d'	Effective electrode separation due to gas flow (cm)
γ	Secondary electron emission coefficient
v_{xm}	Mean velocity of the ambient gas (m/s)
γ_a	Ratio of specific heat at constant pressure to the specific heat at constant volume of the mediating gas.
C_P	Gas specific heat at constant pressure
C_V	Gas specific heat at constant volume

I. INTRODUCTION

We have developed a modified version of Paschen's law [1] that takes into account the flow of gas between electrically charged conductive plates. This model equation makes use of the Mach number and compressible dynamic pressure [2]. This work is applicable to aerospace vehicles traveling through the atmosphere, where they are subject to triboelectrically induced electrostatic charge buildup and possible electrostatic discharge (ESD) damage as a result of dust and ice crystal impingement. Data from preliminary wind tunnel

experimentation at supersonic gas velocities was found to be consistent with the basic premise of the model equations.

II. Theoretical Development

Previously, we have developed a modified version of Paschen's law that incorporates the Mach number and incompressible dynamic pressure terms only [2]. It was subsequently found in our work that for velocities above Mach 0.3 the compressible form of the dynamic pressure term is required. A revised theoretical model was developed using the incompressible dynamic pressure and is presented here.

A. Paschen's Law

Paschen's law, derived in 1889 [1], is an equation that relates the sparking or breakdown voltage between two electrodes to the product of the ambient gas pressure, P, and the electrode separation, d. When the sparking voltage, V_s, is reached, a discharge occurs between the electrodes. Other constant parameters in Paschen's law are the ionization potential of the ambient gas, V_i, atmospheric pressure at sea level, P_{atm}, molecular mean free path at sea level, L, and the secondary electron emission coefficient of the electrode material, γ. Paschen's law is shown in Eq. (1) below [3]. As the electric potential builds up between the electrodes, it affects the small number of electrons and ions typically present in the air (electron-ion pairs). These particles then separate and move towards the oppositely charged electrode. On the way, they can strike and ionize other atoms and molecules thus creating a cascade of charged particles that eventually results in an electrostatic or sparking discharge between the electrodes.

$$V_s = \frac{\frac{V_i}{LP_{atm}}Pd}{ln(Pd) - ln\left[LP_{atm} ln\left(1+\frac{1}{\gamma}\right)\right]} \tag{1}$$

Our hypothesis is that the number of electron-ion pairs created per unit distance is mitigated by the electron-ion pairs removed per unit distance by the flow of gas past the electrodes. In this first approximation, we treat the pressure gradient along the vertical axis (perpendicular to the flow) as a constant. The theoretical equation must be a function of the mean velocity, v_{xm}, of the ambient gas and reduce to Paschen's law, Eq. (1), when $v_{xm} = 0$.

B. Theoretical Model with the Mach Number

Deriving the theoretical model equation with the Mach number as a mitigating factor as before [2] we have

$$V_s = \frac{\frac{V_i}{LP_{atm}}(Pd)}{ln(Pd) - ln\left[LP_{atm} ln\left(1+\frac{1}{\gamma}\right)\right] - M_N} \tag{2}$$

This theoretical model, Eq. (2), is Paschen's Law, Eq. (1), with the Mach number in the denominator. This equation meets the requirement that when $v_{xm} = 0$ it reverts to Paschen's Law.

C. Mach number Formulation with Compressible Dynamic Pressure

When flowing gas is considered there are two components to the pressure P. One is the static or ambient gas pressure, P_0, and the dynamic pressure. The dynamic pressure used previously [2] was the incompressible dynamic pressure.

$$P_{DI} = \frac{1}{2}\rho v_{xm}^2 \tag{3}$$

Here ρ is the gas density and v_{xm} is the mean gas velocity. Total pressure was given by

$$P = P_0 + P_{DI} \tag{4}$$

During the course of this project, we discovered that the compressible form of dynamic pressure must be used above Mach 0.3. Compressible dynamic pressure is given by [4]

$$P_{DC} = P_{DI}\left\{\left[1 + \left(\frac{\gamma_a - 1}{2}\right)M_N^2\right]^{\frac{\gamma_a}{(\gamma_a - 1)}} - 1\right\}\frac{2}{\gamma_a M_N^2} \tag{5}$$

Here γ_a is the ratio of specific heats (for air $\gamma_a = C_P/C_V = 1.4$). The incompressible dynamic pressure, Eq. (3), can be rewritten in terms of γ_a and the Mach number as

$$P_{DI} = \frac{1}{2}\rho v_{xm}^2 = \frac{1}{2}\gamma_a M_N^2 P_0 \tag{6}$$

P_0 is the static pressure. Substituting Eq. (6) into Eq. (5) and collecting terms we have

$$P_{DC} = P_0\left[\left(1 + \frac{\gamma_a - 1}{2}M_N^2\right)^{\frac{\gamma_a}{\gamma_a - 1}} - 1\right] \tag{7}$$

Substituting Eq. (7) into Eq. (2) for the incompressible dynamic pressure factor we have for the sparking voltage in an air gap (now with $P = P_0 + P_{DC}$)

$$V_s = \frac{\frac{V_i}{LP_{atm}}\left[\left(1+\frac{\gamma_a-1}{2}M_N^2\right)^{\frac{\gamma_a}{\gamma_a-1}}\right]P_0 d}{ln\left[\left[\left(1+\frac{\gamma_a-1}{2}M_N^2\right)^{\frac{\gamma_a}{\gamma_a-1}}\right]P_0 d\right] - ln\left[LP_{atm}ln\left(\frac{1}{\gamma}+1\right)\right] - M_N} \tag{8}$$

When $v_{xm} = 0$, Eq. (8) reduces to Paschen's law as required. This equation is graphed in Fig. 1 for stainless steel (SS) electrodes ($\gamma = 0.02$, [5]) at various Mach numbers for air ($\gamma_a = 1.4$) between 0.5 and 3.75 and a gap of 1.3 cm.

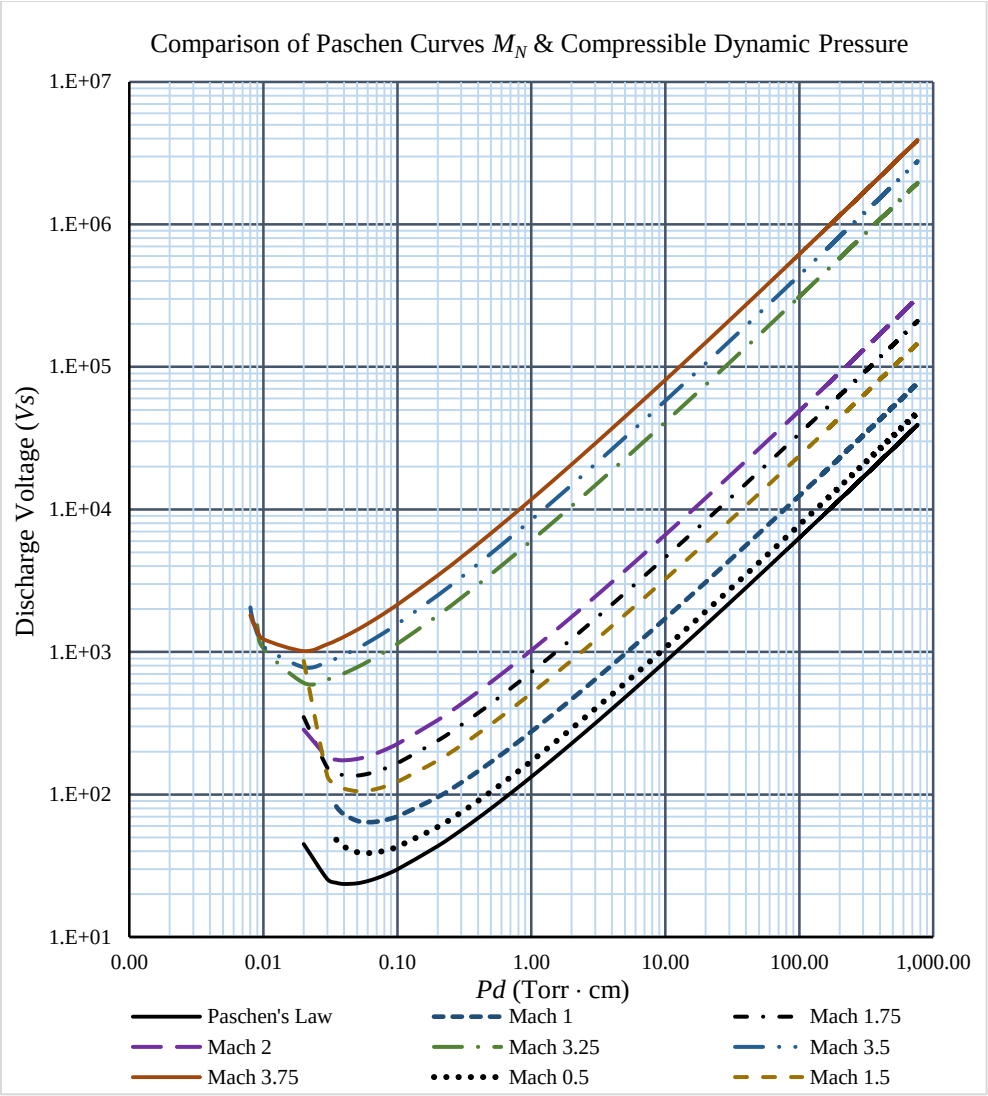

Figure 1. Graphs of the model equation, Eq. (8), for various values of the Mach number. Stainless steel electrodes in air (γ_a = 1.4). All theoretical curves show higher sparking voltages than the Paschen's law curve.

D.An Apparent Effective Discharge Path

When air flows in a channel, a velocity profile is created [4]. This velocity profile is typically parabolic in shape with zero velocity at the channel walls and is maximum at the channel center. Velocity profile data from a Mach 1.47 wind tunnel experiment is graphed in Fig. 3 [7]. This velocity profile is linear across the center of the 4.4 cm wide channel because the length of the test section did not allow for the typical parabolic shape to develop [8].

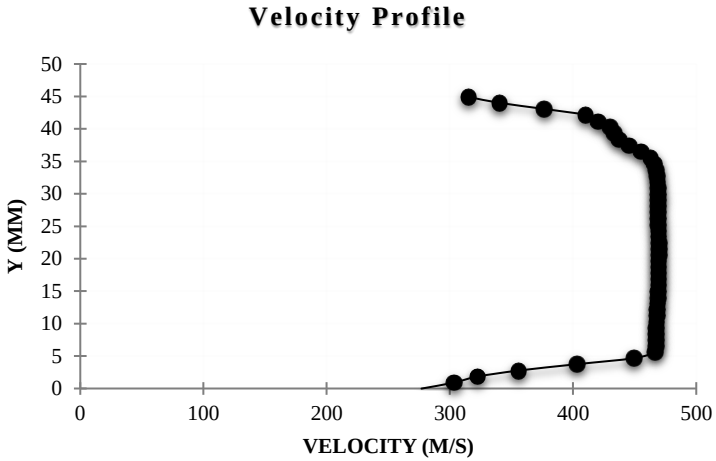

Fig. 3. Wind tunnel data with a channel width of 4.4 cm, a max velocity of Mach 1.47.

Measurement of the distance along the velocity profile in Fig. 3 from a full scale printout gives approximately 11.7 cm. As described before [2], from inspection of Eq. (8) we hypothesize an expression for an effective electrode separation.

$$d' = \left(1 + \frac{\gamma_a - 1}{2} M_N^2\right)^{\frac{\gamma_a}{\gamma_a - 1}} d \tag{9}$$

For air (γ_a = 1.4) at Mach 1.47, we get for Eq. (9)

$$d' = (1 + 0.2 M_N^2)^{3.5} d = 15.48\ cm \tag{10}$$

This gives a value around 30% larger than the 11.7 cm distance graphically measured along the flow profile in Fig. 3. Analysis of other wind tunnel velocity profile data with different channel widths and Mach numbers will be necessary to better evaluate this hypothesis.

III. Experimental Results to Date

Wind tunnel experiments were performed at the Florida Center for Advanced Aero-Propulsion (FCAAP) of the University of Central Florida (UCF) which is a co-investigating organization of this effort. The wind tunnel facility, described previously [2], was modified to allow for sparking discharges inside the test section of the tunnel.

A. Experiment Development

The experiment consisted of one electrode plate placed 1.3 cm below the upper surface of the test section in the wind tunnel. The test section, shown in Fig. 4, was modified to mount the electrode so that the upper stainless steel surface of the test section acted as the ground.

Fig. 4. Wind tunnel showing the test section (clear window on the left) and the internal sting on the right (with a standard aerodynamic cone attached) to which the electrode was mounted in this disassembled view.

The electrode plate was designed by UCF and fabricated by KSC. This plate is made from 304 SS with all edges rounded and surfaces polished to reduce field concentration points. The electrode is 2.0 cm wide by 3.0 cm long with a tapered thickness from 0.32 cm to 0.64 cm. The flat surface of the electrode was positioned to parallel the upper test section surface. A round projection off the end of the flat portion of the electrode was used to mount the electrode onto the test section sting mount and to provide for electrical connection to the power supply. The design of the electrode plate is shown in Figs. 5 and 6. Aluminum was the first electrode metal of choice, but preliminary wind tunnel tests showed that in the electrode configuration required, aluminum deflected too much to keep the gap constant during supersonic flow. A change of material to 304 stainless steel eliminated the deflection problem and also provided the same material for the electrode and ground as the upper surface of the test section is made from 304 stainless steel.

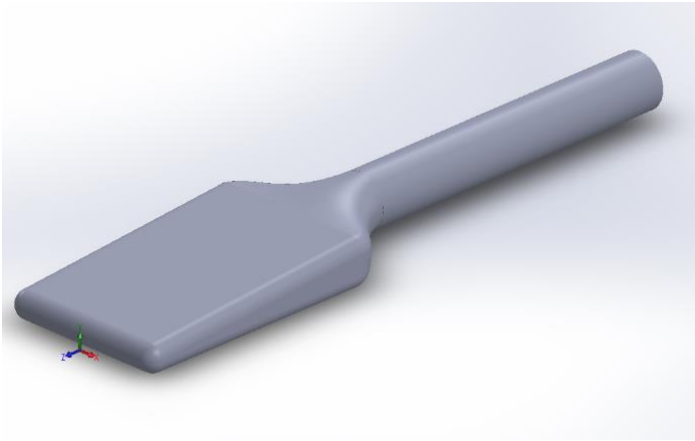

Fig. 5. 304 Stainless steel electrode design.

Fig. 6 304 Stainless steel electrode integrated into the wind tunnel sting mount. The white tube is made from polytetrafluoroethylene (PTFE), which is an insulator. The copper tube provides structural support.

Glassman 10 kV (PS/EH10N10.0-CT) and 60 kV (PS/EH60R01.5) power supplies were used to energize the electrode with the upper surface of the stainless steel test section acting as the ground. Both voltage and current between the electrode and upper test section surface were monitored by a Tektronix DPO 4034 digital phosphor oscilloscope. The UCF facility also had Schlieren flow visualization to determine the shock reflections and pressures around the electrode. Also, for several experiments, discharges were recorded with GoPro™ video of the test section via the side windows. A high-level schematic of this experiment is shown in Fig. 7.

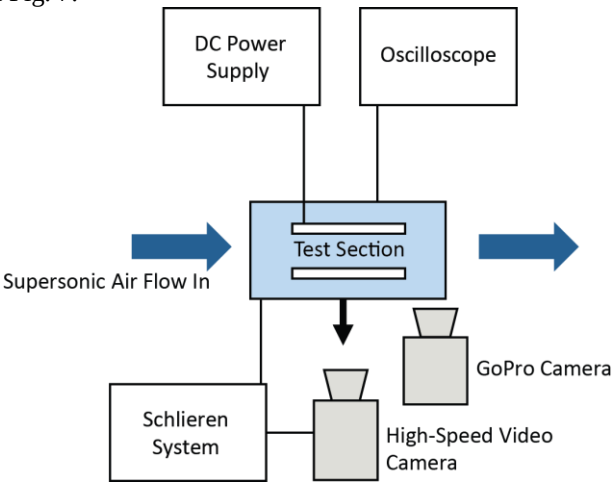

Fig. 7. High level schematic of the wind tunnel experiment to the measure the electrical discharge characteristics of high-speed flow past electrodes.

B. Experiments, Data, and Analysis

Two types of experiments were performed using the apparatus described in Section III-A. One experiment was to start the wind tunnel and, under steady supersonic flow, ramp up the electrode voltage to observe any sparking. The electrode was preloaded to approximately 10 kV, which is below the sparking voltage, so that the ramp span would not be as large. The supersonic steady state condition only lasts for 30 seconds or less, depending on

the air tank pressure and the Mach number. This made it difficult to ramp the electrode voltage in so short a time. Also, the pressure between the electrode and the upper surface of the test section was not fully consistent across the electrode because of shock reflections. Typical shock reflections are visible in Fig. 8, which shows a Schlieren image for the electrode under Mach 3.5 flow.

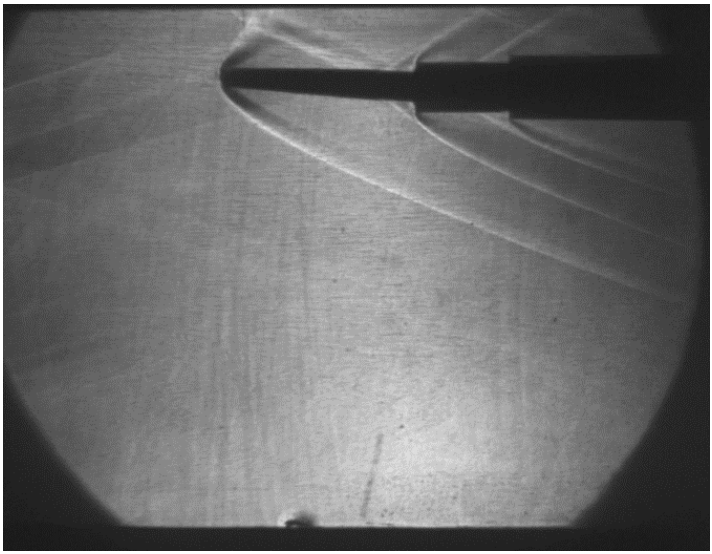

Fig. 8. Schlieren image of Mach 3.5 shock waves and reflections around the electrode. Air flow is left to right.

The second experiment involved preloading the electrode so that it sparked rapidly during no-flow conditions, then turning on the wind tunnel. The sparking would stop as soon as the air reached a sufficient velocity to reduce the number of electron-ion pairs in the gap between the electrode and the upper surface of the test section.

An example of the spark-quenching effect of supersonic air flow is shown in Fig. 9. Here we see the attainment of rapid sparking between the electrode and the grounded upper surface of the test section prior to air flow in panel A (approximately 30 kV), the modification of the spark as air velocity increases in panel B, quenching of sparking in panel C, and the resumption of rapid sparking when air velocity falls at the end of the run.

The wind tunnel apparatus was modified with a more instrumented test section located to the right of the existing test section shown in Fig. 10. Here better measurement of the pressure and air flow in the test section was attained. Many runs were made at Mach 1.65, but only two runs had sparks that were recorded during the supersonic flow portion. These data points are shown in Fig. 11. The data points fit close to the model equation curve (Eq. 7) for air with stainless steel electrodes. Although the experimental results to date are consistent with the hypothesis, more data is required. A follow-on experiment is proposed in section IV.

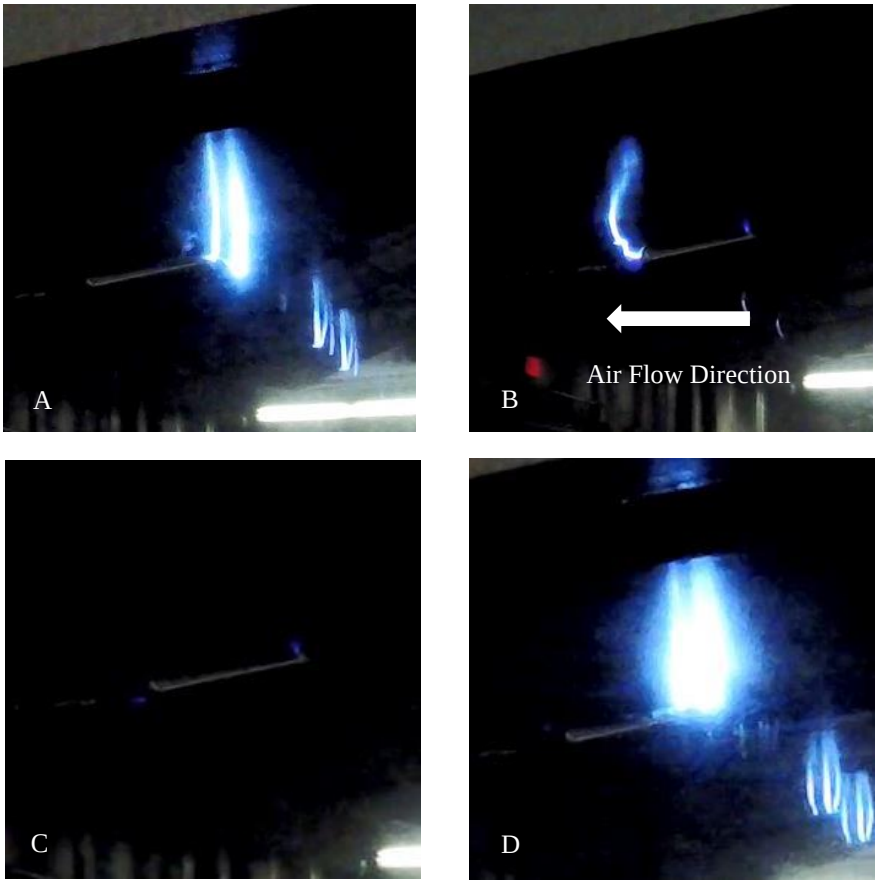

Figure 9. Electrode showing (A) sparking rapidly before onset of air flow, (B) sparks pushed back by initial air flow towards stem of electrode, (C) sparking quenched during supersonic flow, with some small glow discharges still visible, and (D) sparking fully resumed after air flow ceased.

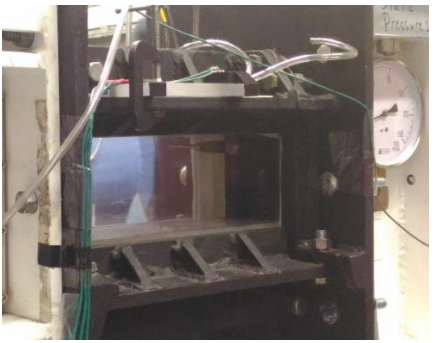

Fig. 10. New instrumented test section for the Mach 1.65 experiments.

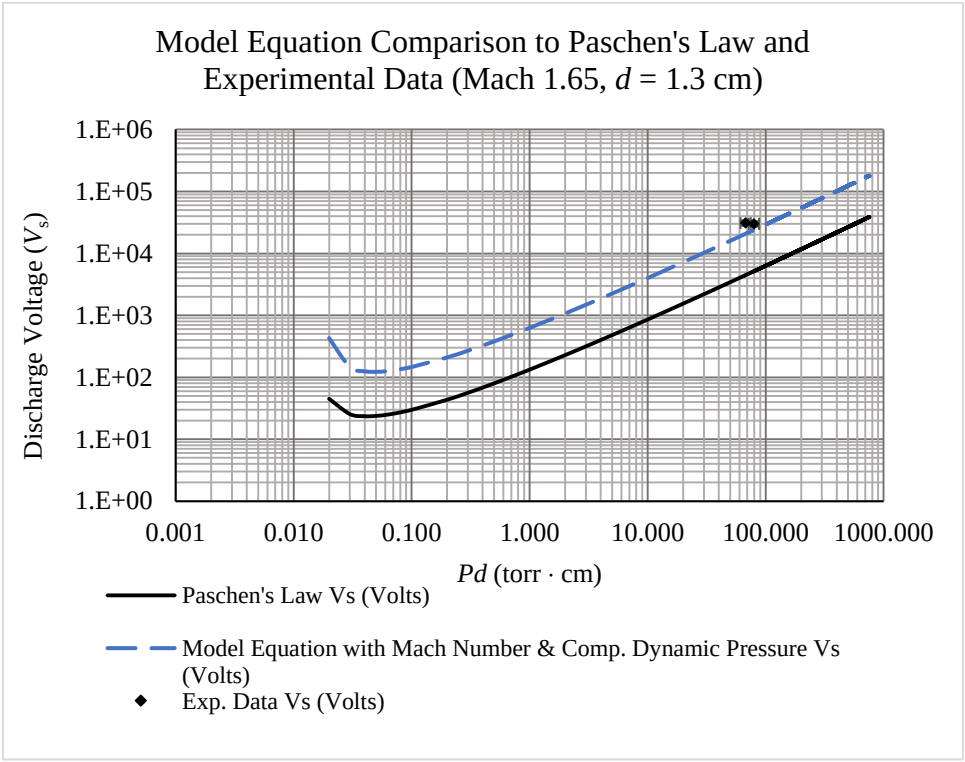

R

Fig. 11. Comparison of Paschen's law for a gap of 1.3 cm to the model equation with Mach number and compressible dynamic pressure terms, Eq. (8), and the two data points obtained for sparking during Mach 1.65 flow.

IV. Future Experiment

Getting reliable pressure and discharge data with the experimental apparatus was found to be very difficult. Future experimental development would be in the form of a specially designed test section where both upper and lower surfaces are the conductive electrodes and can be set at precise separations between 1.0 cm and 2.0 cm. This would allow experimental data to be taken without the shock reflections seen using the current apparatus and give more precise pressure, velocity, and voltage measurements. A notional test section concept is shown in Fig. 12.

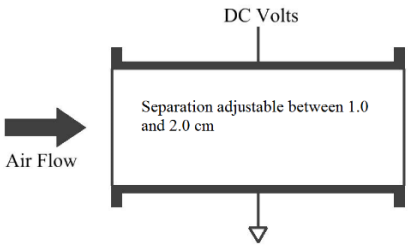

Fig. 12. Schematic concept of the proposed wind tunnel test section with the electrode and ground incorporated into the upper and lower surfaces to reduce shock reflections.

V. Conclusion

In this paper we have presented a re-derivation of Paschen's law that takes into account the flow of gas between the electrodes as a mitigating factor on the concentration of electron – ion pairs created by the potential. Aerodynamic properties such as the Mach number and dynamic pressure were used in this re-derivation and returned higher values of V_s, as would be expected if the concentration of electron – ion pairs were reduced by a rapid gas velocity. Experimental results obtained to date are consistent with this hypothesis though more experimentation is required. Also, in a gas flow between the electrodes, an effective discharge distance was hypothesized to be the length of the resultant velocity profile across the test section channel. Further evaluation of this hypothesis is planned with larger and improved wind tunnel data sets.

Acknowledgements

The authors would like to thank the NASA Science Innovation Fund (SIF) for their support of this work. Also special thanks to Dr. Carlos Calle, Mr. Michael Johansen, Mr. James Phillips, and Mr. Paul Mackey of the NASA Electrostatics and Surface Physics Laboratory (ESPL) at the Kennedy Space Center for their reviews and helpful comments on this paper.

References

[1] Friedrich Paschen "Ueber die zum Funkenübergang in Luft, Wasserstoff und Kohlensäure bei verschiedenen Drucken erforderliche Potentialdifferenz (On the potential difference required for spark initiation in air, hydrogen, and carbon dioxide at different pressures)". Annalen der Physik **273** (5): 69–75 (1889). *Bibcode:1889AnP...273...69P*. *doi:10.1002/andp.18892730505*.

[2] M. Hogue, et. al., "Dynamic Gas Flow Effects on the ESD of Aerospace Vehicle Surfaces", Proceedings, ESA Annual Meeting 2016.

[3] A. Von Hippel, *Molecular Science and Molecular Engineering*, (MIT Press, Wiley & Sons, 1959), pp 39-47.

[4] Sultanian, Bijay, Fluid Mechanics: An Intermediate Approach, N.P.: CRC, n.d. Print, p. 33.

[5] J. D. Cobine, *Gaseous Conductors: Theory and Engineering Applications*, Dover, 1993, p. 159, Table 7.3.

[6] http://www.uio.no/studier/emner/matnat/math/MEK4450/h11/undervisningsmateriale/modul-5/Pipeflow_intro.pdf

[7] Velocity profile data provided by Dr. K. Ahmed/UCF, 2-17-2016.

[8] R. W. Fox, A. T. McDonald, *Introduction to Fluid Mechanics*, 2nd ed., John Wiley & Sons, 1978, p. 496.